Visual Abstract

Influence of manufacturing shrinkage and microstructural features on the strength properties of carbon fibers/PEEK composite material

E.V. Lomakin, B.N. Fedulov
Department of Mechanics and Mathematics, Lomonosov Moscow State University, Russia
evlomakin@yandex.ru, http://orcid.org/0000-0002-8716-5363
fedulov.b@mail.ru, http://orcid.org/0000-0002-1894-5964

A.N. Fedorenko
Center for Materials Technologies, Skolkovo Institute of Science and Technology, Russia
alexey.n.fedorenko@gmail.com, https://orcid.org/0000-0002-3260-7531

ABSTRACT. This research discusses the micromechanical modelling for thermoplastic composite material. Elastoplastic and damage model for PEEK matrix composite with the dependency of properties to stress state is presented. Plasticity initiation conditions and failure criterion are analyzed. The influence of manufacturing residual stresses is considered. All typical engineering experiments for neat PEEK under different stress state are good predicted by the model. Numerical experiment for macro-properties estimation based on micromechanical model is conducted and the results are compared with the test data.

KEYWORDS. Composites; Micromechanics; PEEK matrix; Mechanical properties.

OPEN ACCESS

Citation: Lomakin, E. V., Fedulov, B. N., Fedorenko, A. N., .Influence of manufacturing shrinkage and microstructural features on the strength properties of carbon fibers/PEEK composite material, Frattura ed Integrità Strutturale, 62 (2022) 527-540.

Received: 08.07.2022
Accepted: 09.09.2022
Online first: 12.09.2022
Published: 01.10.2022

INTRODUCTION

The modelling of cracking and failure of fiber-reinforced composites is challenging due to their inherent heterogeneity and numerous damage modes. On the macro-level, it is possible to represent every composite layer as anisotropic homogenized solid, and to combine continuum damage model for intra-laminar failure [1,2] with a cohesive zone model (CZM) for inter-laminar cracking [3]. While different techniques were proposed for the application of cohesive elements in finite element model (FEM) [4,5], the main disadvantage is the restriction of cracking only along predefined trajectories. An extended finite element model (XFEM) allows the simulation of crack propagation in arbitrary direction [6,7]. Due to the computational costs, alternative numerical methods were developed, i.e. based on floating node method with cohesive elements inserted in front of the crack tip [8].

On the other hand, the analysis on the micromechanical scale allows to clarify the homogenized macro properties [9] and to understand failure mechanisms. Development of FEM for representative volume element (RVE) requires generation of realistic random fiber distributions [10,11] and special numerical technics for periodic boundary conditions [12]. Fiber is usually assumed the elastic material, while elastoplastic matrix properties play a key role in the analysis.
A prediction of intralaminar material properties and in-plane non-linear shear behavior has performed in [13] based on periodic RVE. Sun et al. [14] developed failure criteria of unidirectional fiber-reinforced composite under different loading conditions. Chen et al. [15] studied the influence of loading path on the failure of composite laminae. Yuan et al. [16] proposed a model of RVE failure under shear load for the fracture toughness estimation, and the result is driven by matrix plastic and damage characteristics. Micromechanical simulation of matrix cracking is presented in [17] for transverse load of carbon/epoxy RVE. Varandas et al. [18] performed micromechanical simulation of mode I test for IM7/8552 carbon-epoxy composite laminate, including the analysis of different layup sequences. RVE-based analysis was used for fatigue properties estimation in [19]. Micromechanical approach for failure of composites undergoing large deformation is presented in [20].
The use of matrix nominal properties is not always appropriate for the simulation, since real properties of polymer matrix depend on different factors, such as degree of crystallinity [21] or residual stresses [22–25]. Manufacturing imperfections such as temperature inhomogeneity is usual for real industrial products, this causes discrepancy in crystallization and matrix shrinkage, and these consequently modify mechanical properties. For example, Li et al. [26] reported lower strength prediction with the use of matrix properties measured directly from the tests of standard specimens at the macroscale level, and the calibration procedure was proposed to match the experimental results. Vaughan and McCarthy [27] found that thermal residual stress compensate tensile stresses developed under transverse tensile loading with the increase of overall RVE strength. They also altered properties of fiber–matrix interface and found that it significantly influences on the RVE strength.
In the presented study the RVE for carbon fiber/PEEK unidirectional lamina is developed for the strength estimation under transversal load. Since it is difficult to measure interface properties, the fiber–matrix interface is not considered in micromechanical model. Also as an assumption, we used perfect PEEK material with maximum degree of crystallinity. Similarly with the published results [26], a certain inconsistency with experimental strength value was found using properties for the model directly from material datasheet. In particular, damage initiates in a narrow area between fibers located close to each other, so damaged area propagates rapidly from these localizations causing underestimation of total RVE strength. This effect cannot be eliminated only by correction of matrix plasticity limits due to the need of fit the value of failure strain simultaneously. Thus, the manufacturing residual stress is considered as a factor, which compensates premature damage in weak regions and at the same time allows to match correct total failure strain of RVE.

MATERIAL PROPERTIES

In spite of understanding that thermoplastic materials and polymers in general have complex mechanical properties, there is a lack of extensive experimental research even for such a popular material as PEEK. Considering datasheets [28-29] from PEEK manufacturers and the properties analysis made in [30], it is possible to conclude, that isotropic linear elasticity gives relatively good approximation under small deformations conditions. The corresponding elastic constants for neat PEEK material are shown in Tab. 1. Plasticity modelling has no well-adopted approach for such material, but following [30], it is possible to conclude that plasticity initiation criterion is supposed to be pressure dependent. Fig. 1 shows some plasticity initiation points, performed in chart with equivalent von Mises stress versus first invariant of stress tensor ($\sigma=1/3\sigma_{ii}$). Good approximation for presented data gives the linear curve, which corresponds to Drucker-Prager criterion (1). Middle drop of shear data is neglected, mostly due to convenience of usage simple standard plasticity model, which is built into ordinary FEM software. Probably the main reason for this drop at shear experiment is the complexity of determination of the true plasticity initiation point. Because nonlinearity for shear loading diagram can be partially connected with nonlinear elastic stage of deformation, which is usually neglected.

$$\sigma_0 + C\sigma = k\left(\varepsilon_{eq}^{pl}\right) \tag{1}$$

where ε_{eq}^{pl} -equivalent plastic strain, σ and σ_0 are the hydrostatic component of stress and equivalent von Mises stress correspondingly, $k\left(\varepsilon_{eq}^{pl}\right)$ – experimental hardening function, C – experimental constant ($C=\tan\varphi$, φ – dilatation angle).

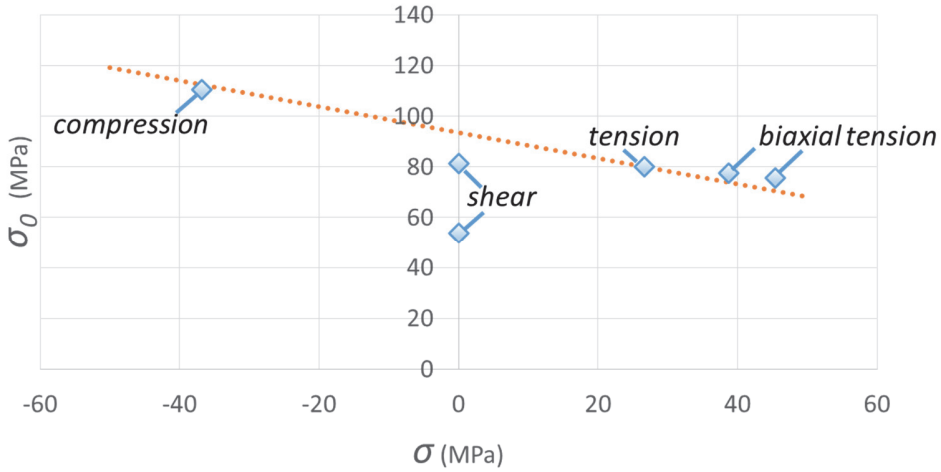

Figure 1: Plasticity limits for different type of loadings in terms of Mises stress vs hydrostatic component of stress [30]

Mechanical constants		Tensile hardening	
Modulus, GPa	3.6	σ_t^{pl}, MPa	ε_{eq}^{pl}
Poisson ratio	0.3	77	0
k_0, MPa	89.8	81	0.1
C	0.5	100	0.5
φ, °	27	101	2

Table 1: Mechanical constants for PEEK material modelling

For failure criterion, we need to do some assumptions. The main idea is to have 70% elongation at failure in case of uniaxial tension [29] and much more for compressive types of loading. For this reason, Kolmogorov's criterion [31, 32] (eq. 2) is used with parameters shown in Tab. 2. It has 70% for uniaxial tension stress state and linear growth up to 150% for compressive one, which is purely an assumption.

$$D^{pl} = \int \frac{d\varepsilon_{eq}^{pl}}{\varepsilon_D^{pl}(\xi)} \tag{2}$$

where $\varepsilon_D^{pl}(\xi)$ –determined experimentally piecewise linear function, $\xi = \sigma / \sigma_0$ – stress triaxiality parameter, $D^{pl} = 1$ is the failure criterion.

In addition, the criterion (2) data for neat PEEK material has decay of failure strain for tensile types of loadings, where triaxiality parameter goes to biaxial and triaxial area ($\xi > 1/3$). Fig. 2 shows how Abaqus program treats data taken from Tab. 2. Last and first points have horizontal plateau for out of the table range of triaxiality parameter. It must be underlined that for failure we have only one experimental point for uniaxial tension experiment, the rest of them is the assumption. Experimental point has a grey background in Tab. 2 and underlined in chart shown in Fig.2.

Tabs. 1 and 2 show all necessary data required for standard modelling of PEEK polymer in most FEM programs.

Using properties for thermoplastic matrix material assembled in Tab. 1. and AS4 fiber properties shown in Tab. 3, the plane strain problem with uniaxial tension of periodic RVE was realized using FEM Abaqus program.

Failure criterion	
Triaxiality, ξ	Strain at failure, ε_D^{pl}
-0.333	1.5
0	1
0.333	0.7
0.495	0.55
0.666	0.4
1	0.2

Table 2: PEEK failure criterion data used in the analysis.

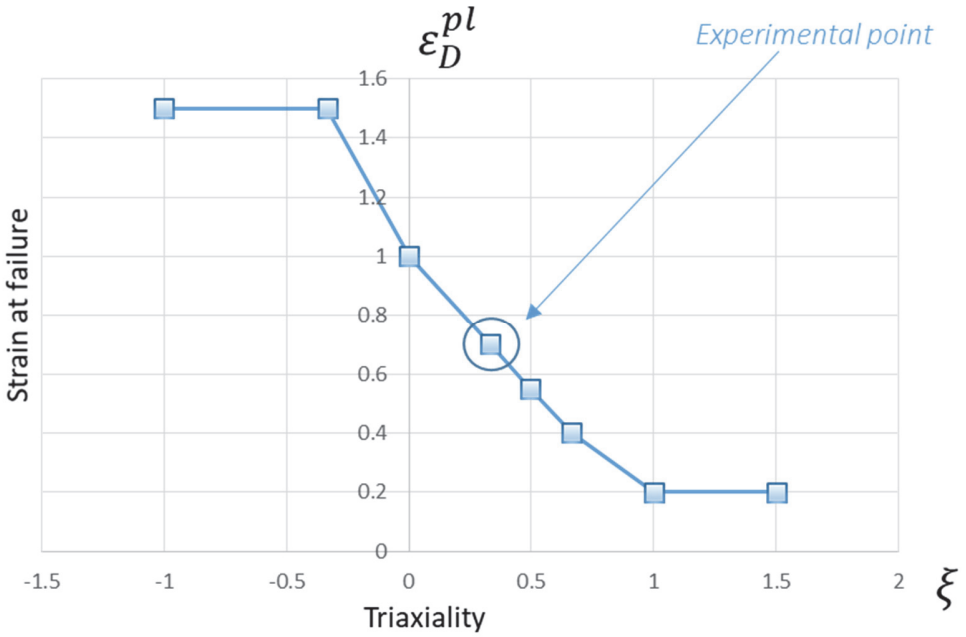

Figure 2: Failure criterion data for PEEK material

E_1 (GPa)	$E_2 = E_3$ (GPa)	$G_{12}=G_{13}=G_{23}$ (GPa)	$\nu_{12}=\nu_{13}$	ν_{23}
235	13.2	27.6	0.2	0.5

Table 3: AS4 carbon fiber properties used in the model [30].

CONSTITUTIVE RELATIONS FOR PEEK MATERIAL

Tab. 4 shows constitutive equations used for matrix material modelling. All relations including elasticity, plasticity and damage have standard implementations into FEM Abaqus program.

Elastic relations:	
$\sigma_{ij} = E_{ijkl}\varepsilon_{kl}^{el},$ $E_{ijkl} = \frac{\nu E}{(1+\nu)(1-2\nu)}\delta_{ij}\delta_{kl} + \frac{E}{2(1+\nu)}\left(\delta_{ik}\delta_{jl} + \delta_{il}\delta_{jk}\right)$	Isotropic linear elasticity
Plasticity active process:	
$\sigma_0 + C\sigma = k\left(\varepsilon_{eq}^{pl}\right)$	Plasticity initiation criterion
$F\left(\sigma_{ij}\right) = \sigma_0 + C\sigma$	Plasticity potential
$\varepsilon_{eq}^{pl} = \int \frac{\sigma_{ij} d\varepsilon_{ij}^{pl}}{\sigma_0 + C\sigma}$	Equivalent plastic strain
$d\varepsilon_{ij}^{pl} = d\lambda \frac{\partial F}{\partial \sigma_{ij}}$	Associated plastic flow theory
Damage model:	
$D^{pl} = \int \frac{d\varepsilon_{eq}^{pl}}{\varepsilon_D^{pl}(\xi)},$	Plasticity initiation criterion
$D^{pl} = 1$	Failure criterion
$E = \begin{cases} E^0, 0 \le D^{pl} < 1 \\ 0, \ D^{pl} = 1 \end{cases},$	Stiffness immediately becomes zero when failure criterion is satisfied.
E^0 – *initial Young modulus*	

Table 4: Constitutive equations used for PEEK material modelling.

RVE MODEL

Fig. 3 shows the plane strain model for representative volume element (RVE). Model has 52000 reduced integrated elements of type CPE4R in Abaqus notation. Composite consists of ~60% volume of fibers and the rest is the PEEK matrix material. Fiber diameter is 5.2μm. Model uses periodic boundary conditions with displacement loading (3) [30].

$$\begin{aligned} &u_1(x+L) = u_1(x) + \varepsilon L, u_2(x+L) = u_2(x) \ \forall x \in \partial\Omega_1 \cup \partial\Omega_3 \\ &u_1(x+L) = u_1(x), \ u_2(x+L) = u_2(x), \forall x \in \partial\Omega_2 \cup \partial\Omega_4 \end{aligned} \tag{3}$$

where u_i – displacement components, L- side length of RVE, ε – applied uniaxial strain, x – point, $\partial\Omega_{1,2,3,4}$ – RVE boundaries

Right part of the Fig. 3 shows that composite cell has a periodic structure for both in-plane directions.

Due to convergence problems, explicit solver with double precision was used for modelling. Time period with linear loading growth was chosen as 1 sec. This time period gives loading rate that coincidences with the static analysis up to possible convergence.

Fig. 4 shows tensile loading curve for composite material, which corresponds to transversal loading. Loading curve fits well elastic slope and strength limit provided by manufacturers [28-29]. Nevertheless, modeling result has a wide diagram and almost doubles strain at failure, experimental one is 0.88% versus modelling result with failure strain of 2%. Almost all parameters in performed model are frozen by experimental data with basic experiments with neat matrix material. Only failure criterion points are free to modify, except pure uniaxial tension (experimental tensile failure strain 70%). Variations

of free points in failure criterion does not reduce failure strain for composite material remaining the high strength (experimental transversal tensile strength 86 MPa).
These numerical results make authors to think about what the feature of developed cell of composite material is missed. The idea of taking into account the residual stresses appeared during composite manufacturing can change the picture of the material deformations.

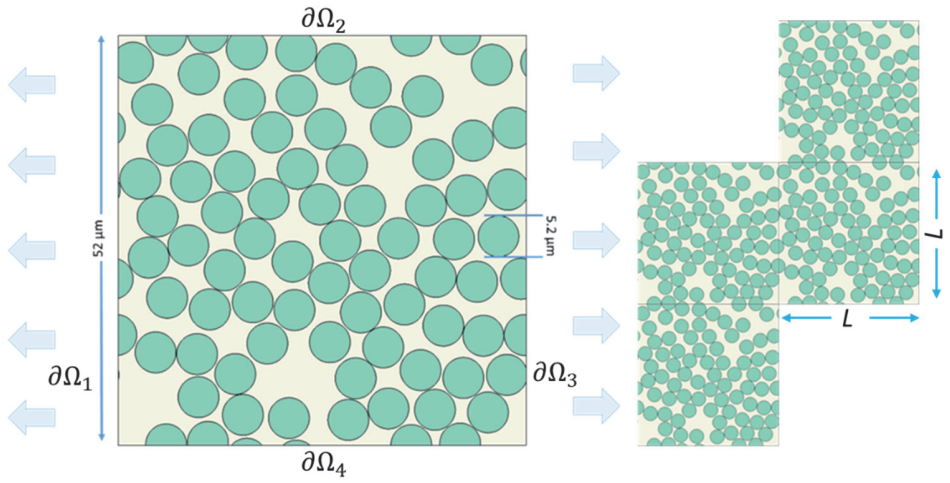

Figure 3: Model for RVE

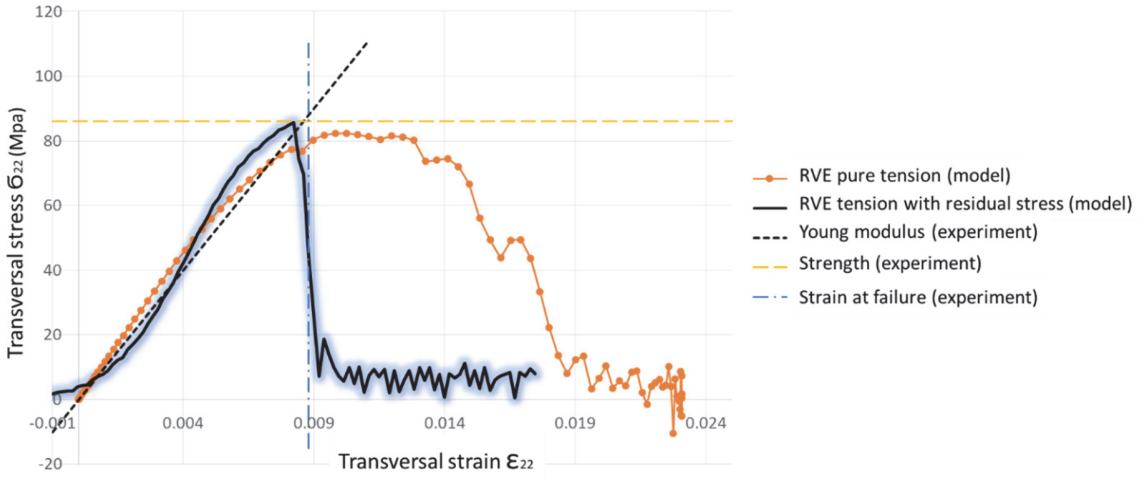

Figure 4: Loading diagram for transversal tension of composite material

The total shrinkage of the PEEK polymer is 15% [33], but even if this volume deformations appeared at very soft stage of the matrix material it cannot cause essential residual stresses. Only half of PEEK manufacturing shrinkage takes place when glass temperature is reached. Applying to matrix material the shrinkage of 7.5% damages RVE of composite seriously. The problem is that no modifications due to high temperature and low crystallinity were taken into account in performed model. High temperature reduces plasticity limit and Young modulus values. Low crystallinity values also reduce limit of plasticity and Young modulus but extremely increases failure at strain characteristic for neat PEEK polymer. Moreover, high level deformations can destroy developed crystals and reduce crystallinity but new internal crystals can be formed at high temperature based on deformed state what "heals" the material and increases its mechanical characteristics. Nevertheless, usage of manufacturing shrinkage reduces strain at failure for performed model. Using material model for PEEK without any modifications, the shrinkage was reduced to 3% to capture effect of 0.88% strain at failure. This value of 3% for not modified properties can be treated as effective shrinkage to get a correct residual stress for composite material. Moreover, adding the manufacturing stresses to performed model causes loading curve to get exactly 86 MPa of tensile strength, which perfectly coincides with experimental data (Fig. 4).

The proximity of loading diagrams to initial stiffness, strength and strain at failure verifies the performed model and all the assumptions mostly made for failure input data, too.

Figs. 5-7 show some stress and strain parameters caused by manufacturing shrinkage. It must be noted, that the highest plastic strain areas are concentrated around fibers, and at places where the fibers placed close to each other Fig. 7. The reason is negligibly small shrinkage of fibers due to high manufacturing temperatures.

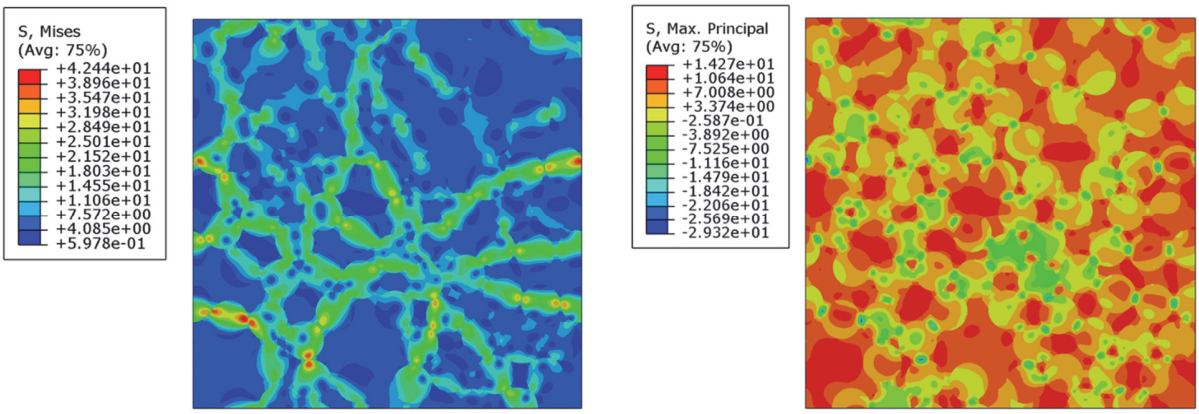

Figure 5: Residual von Mises stress (left), Max principal stress(right), MPa

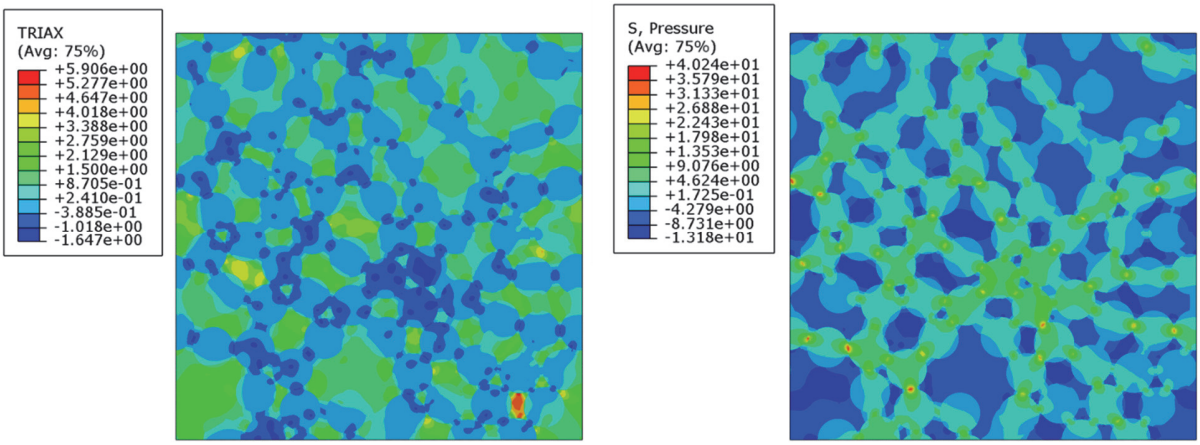

Figure 6: Residual stress MPa, Triaxiality (ξ) (left), Pressure ($-\sigma_{ii}$) (right), MPa

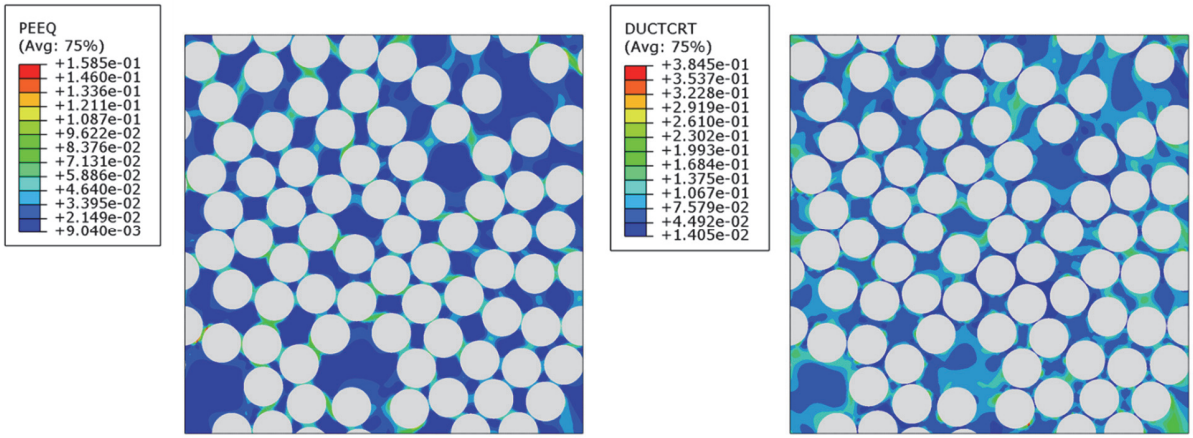

Figure 7: Equivalent plastic strain $\left(\varepsilon_{eq}^{pl}\right)$ (left), damage parameter (D^{pl}) (right), MPa

Triaxiality parameter distribution in RVE model varies from values corresponding to triaxial compression to triaxial tension. It is possible to see that big areas of matrix material are under tensile stress states and areas between fibers are under triaxial compression conditions (Fig.6). The highest-pressure values are placed in the very narrow areas between fibers. Fig. 8 shows maximum principal stress component and its directions. It is possible to see that maximum principal stress component is positive everywhere except narrow areas between fibers. It can be explained by attraction of fibers to each other by regular wide zones of matrix material, which have shrinkage during manufacturing. Narrow areas between the fibers consequently are compressed by neighbor fibers (Fig. 8).

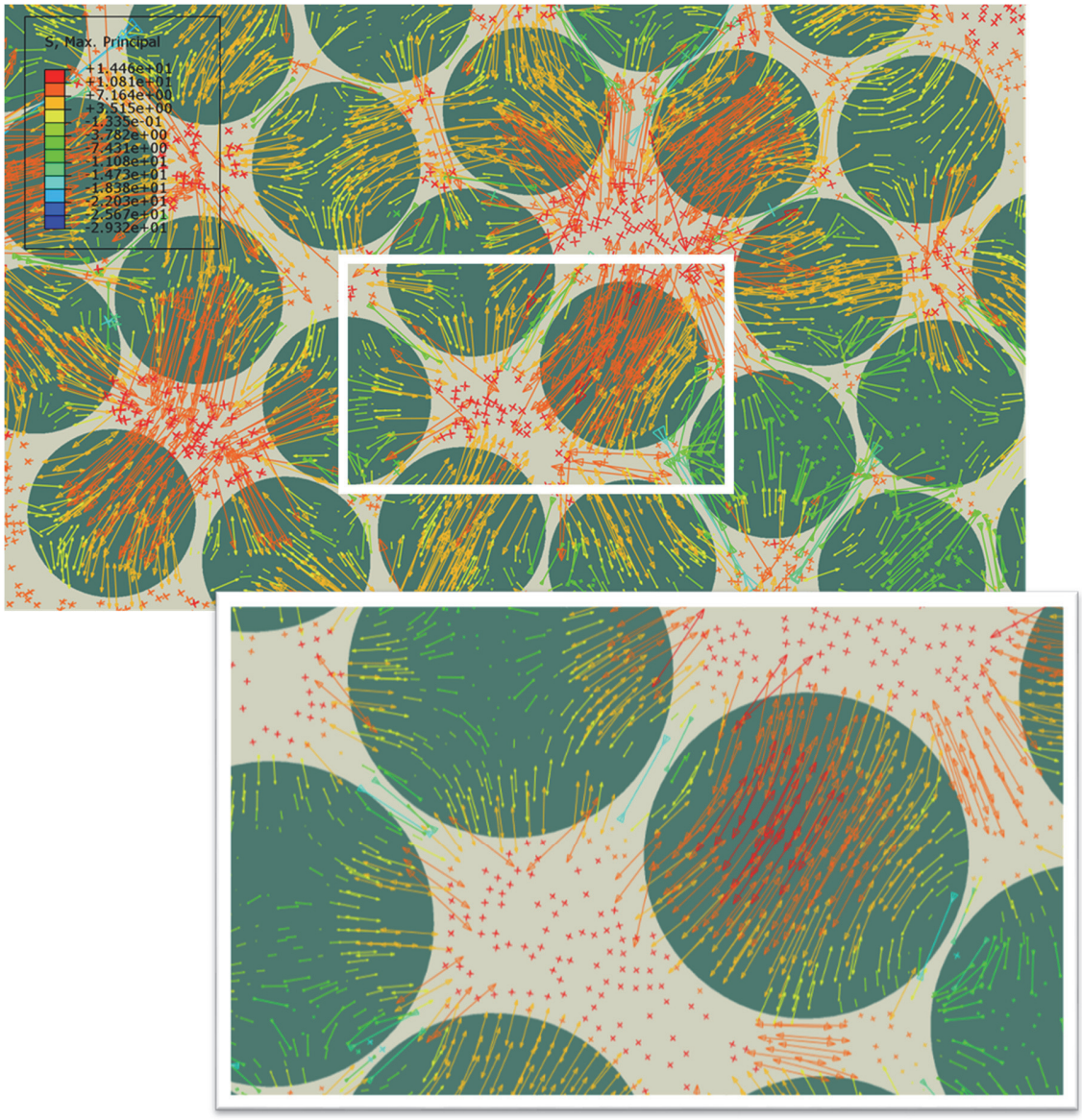

Figure 8: Residual stress MPa, max principal.

This situation is well explained by out of plane stress component σ_{33} distribution – Fig .9. Wide far away from fibers areas (noted as 1 in Fig. 10 c) have a positive stress along fiber direction and negative stress presents in the areas where fibers come close to each other (noted as 2 in Fig. 10 c). Fibers squeeze matrix material in plane and due to Poisson's effect matrix extends in out of plane direction along fibers, that cause compressive stress. Fig. 10 shows equivalent plastic strain between close arranged fibers and its maximum value does not correspond to the maximum of the damage parameter D^{pl} , because this plastic strain caused by compressive stresses, which according to performed failure criterion (2) in combination with Tab. 2 input data generates less damage.

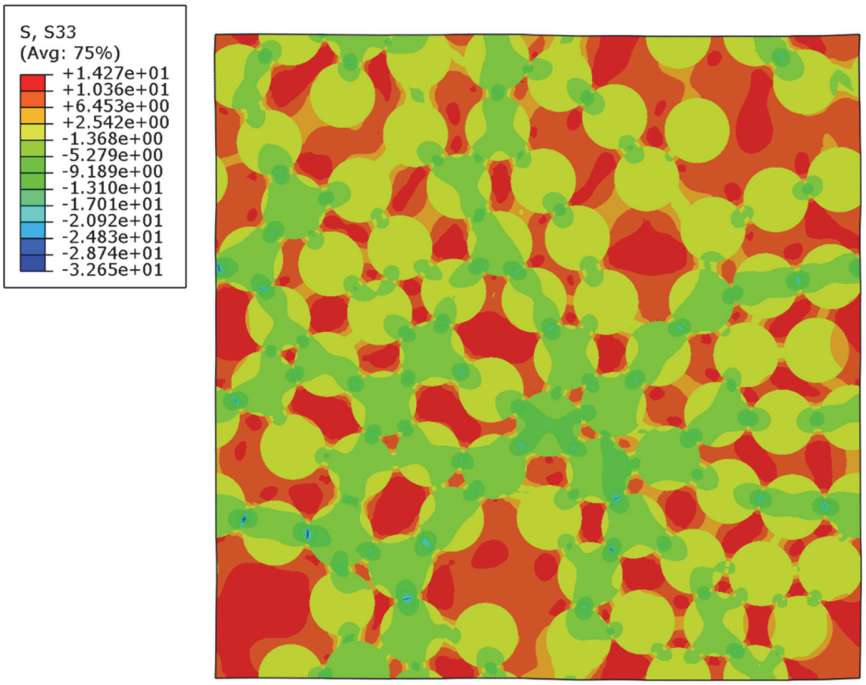

Figure 9: Residual stress MPa, out of plane stress component σ_{33}.

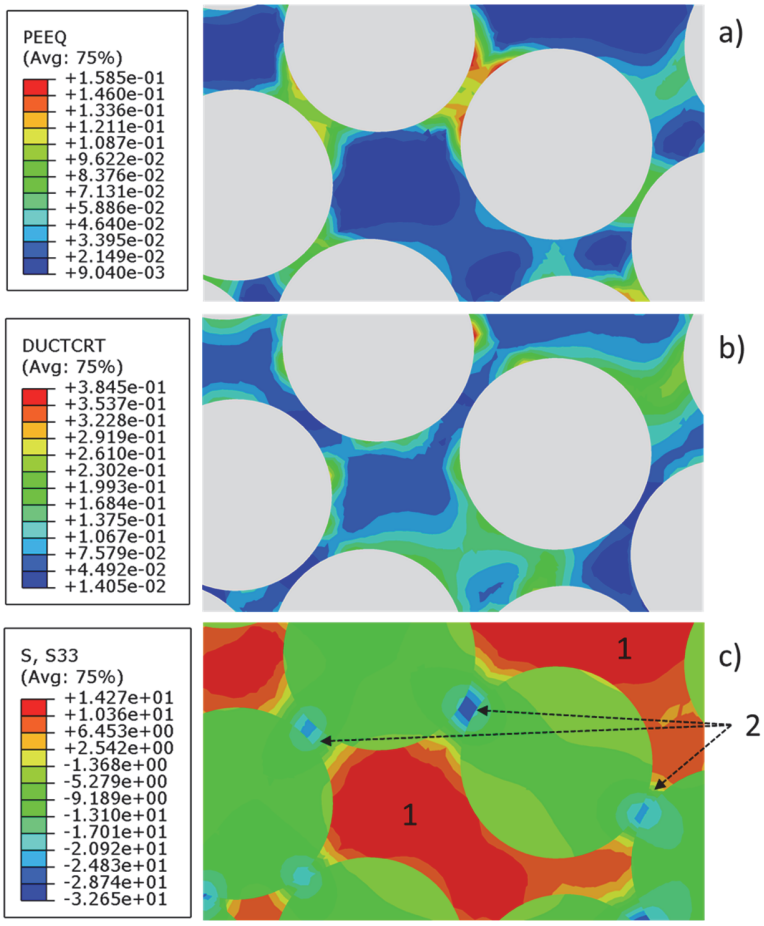

Figure 10: a) equivalent plastic strain $\left(\varepsilon_{eq}^{pl}\right)$, b) damage parameter (D^{pl}), c) Residual stress MPa, out of plane stress component σ_{33}.

Next Figs. 11-17 show the results of modelling of tension of developed RVE. All figures grouped into two categories with maximum stress achieved during loading and maximum strain to see the final failure. In all figures, the left pictures correspond to the loading with no residual stress, and the right ones show the results with manufacturing shrinkage preloading.

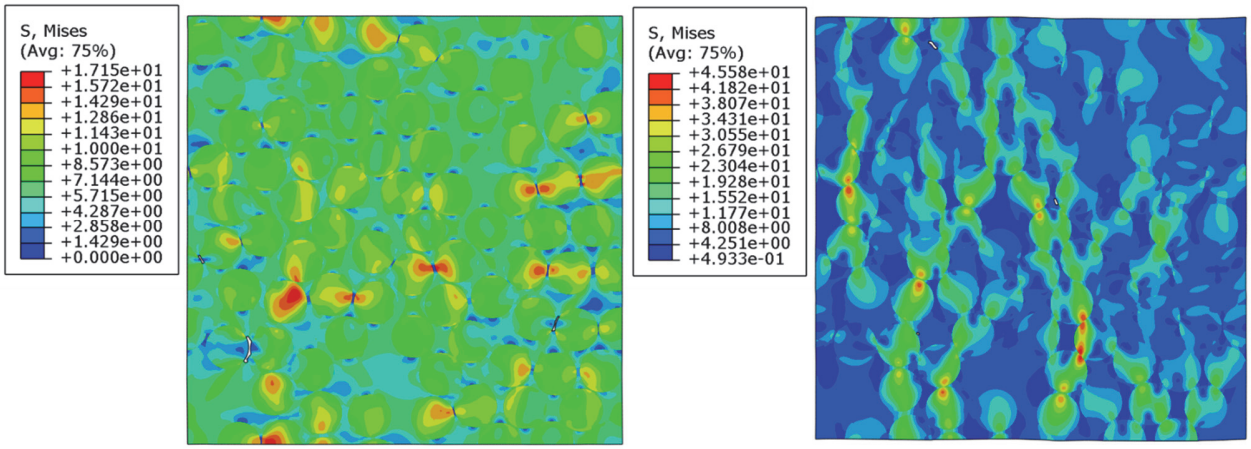

Figure 11: von Mises stress, MPa (pure tension on the left, tension with residual stresses on the right).

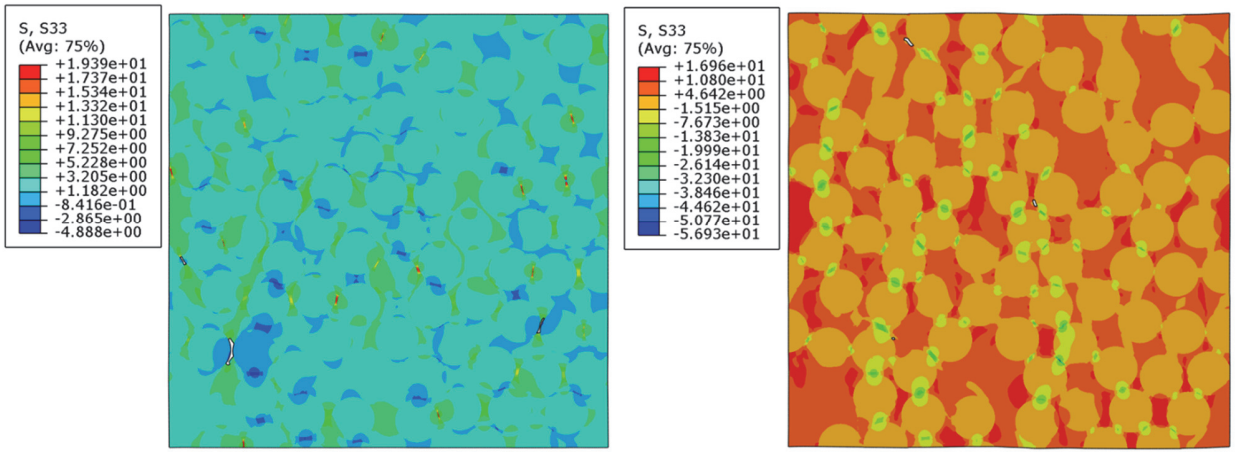

Figure 12: Out of plane stress component σ_{33} at strength stress, MPa (pure tension on the left, tension with residual stresses on the right).

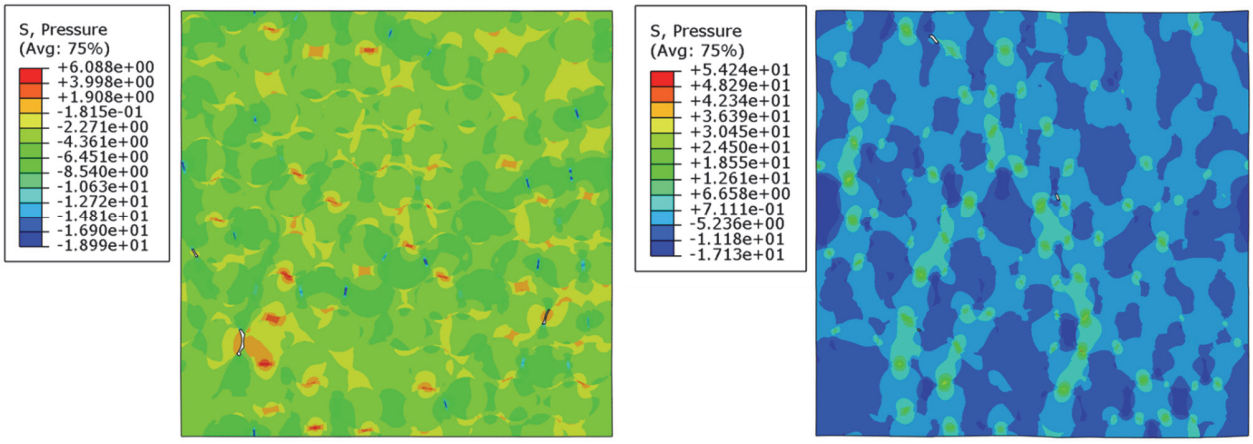

Figure 13: Pressure ($-\sigma_{ii}$) at strength stress, MPa (pure tension on the left, tension with residual stresses on the right).

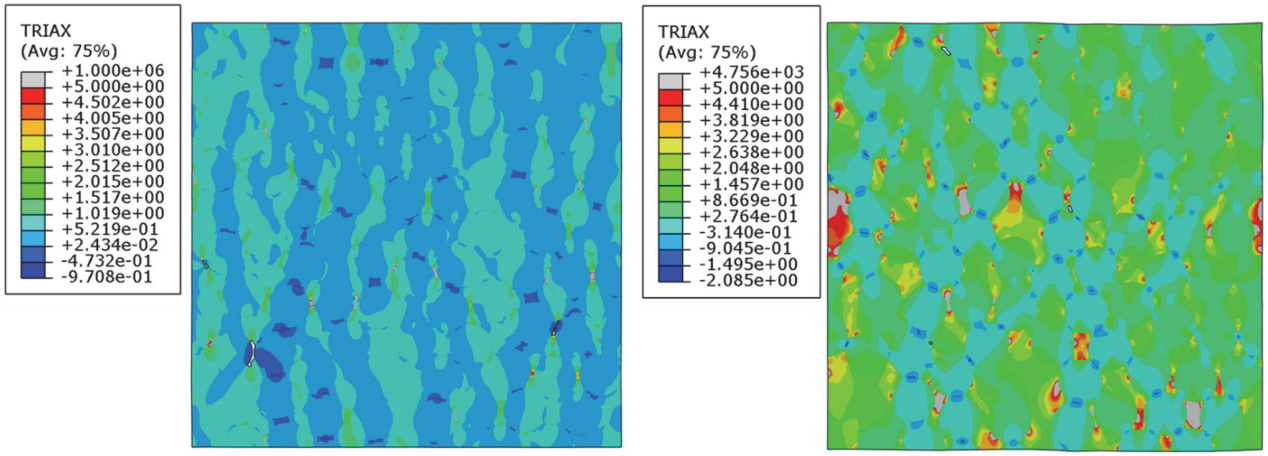

Figure 14: Triaxiality (ξ) at strength stress (pure tension on the left, tension with residual stresses on the right).

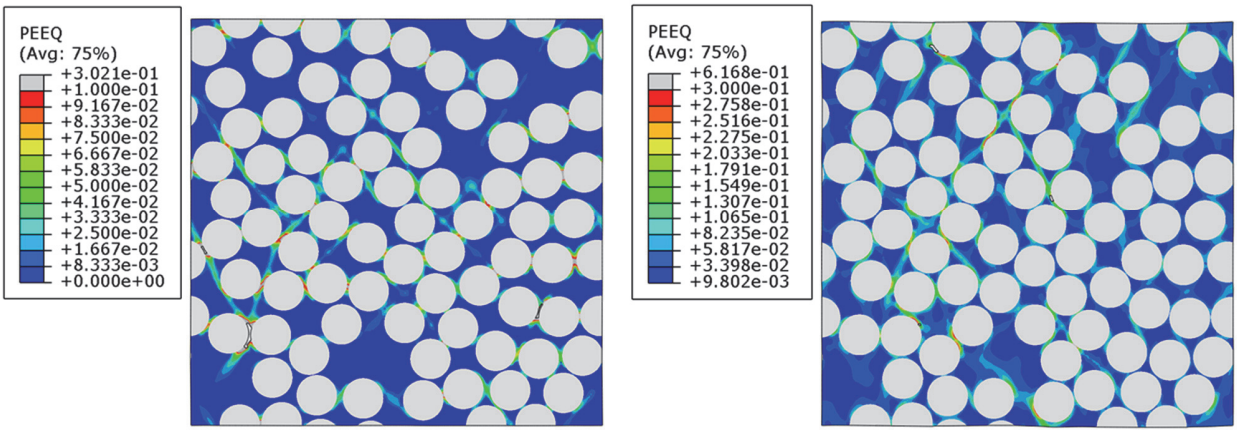

Figure 15: Equivalent plastic strain $\left(\varepsilon_{eq}^{pl}\right)$ at strength stress (pure tension on the left, tension with residual stresses on the right).

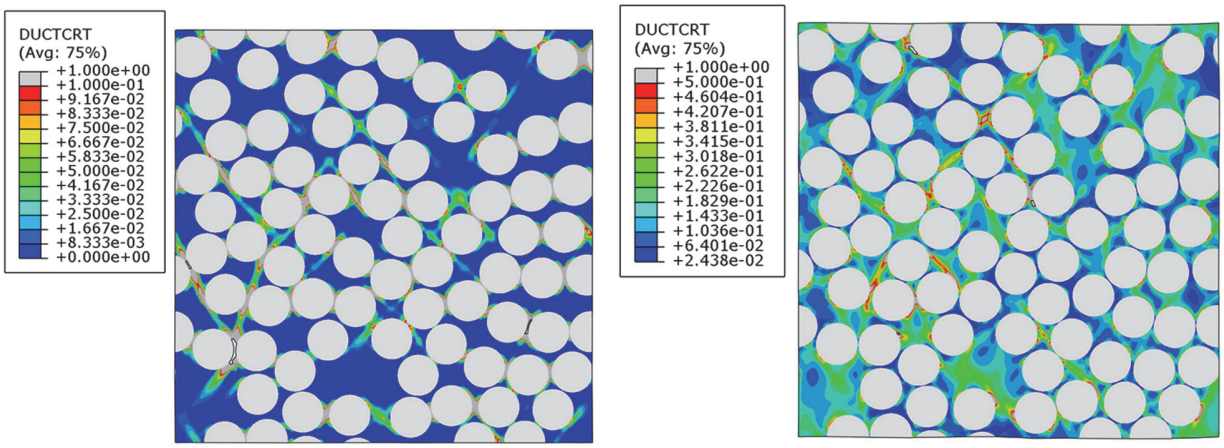

Figure 16: Damage parameter (D^{pl}) at strength stress (pure tension on the left, tension with residual stresses on the right).

Fig. 17 shows the development of damage parameter with appearing of crack inside the composite material. The model without residual stresses has localized damage areas, while RVE with manufacturing stresses has a wider distribution of damages during tension. This can explain a rapid load drop after the limit strength is achieved (Fig. 3). Small raise of the strength for preloaded RVE, which is 5%, explained by the initial compressed stress states of the weakest points in the composite material, which are narrow areas of the matrix between fibers, which caused by manufacturing residual stresses. Also with some additional runs, strain growth was stopped after some cracks appeared. This caused crack growth to stop, what means that the matrix cracking process is stable.

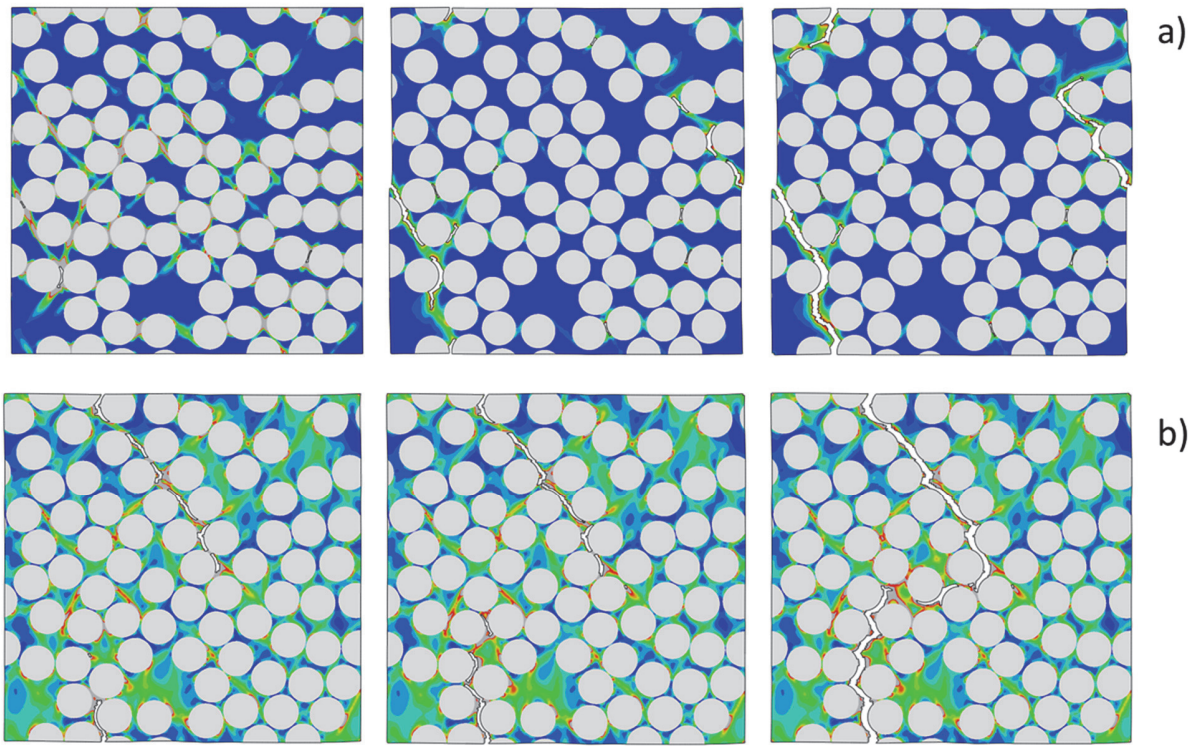

Figure 17: Damage evolution (D^{pl}): pure tension (a), tension with residual stresses (b)

Discussion

The analysis of results shows that the weakest zones in composite structure are the narrow layers where matrix material is clamped between fibers. In these areas, the significant compressive plastic deformations are formed. The technological shrinkage of PEEK matrix causes the raise of compressive plastic strains, but under tensile loading conditions the strains have opposite sing. Taking into account the residual technological shrinkage stresses, under tensile loading these deformations are summarized and graded into one another, thus the material becomes more strengthened.

Conclusion

The material model for PEEK polymer has been provided. It has been verified on the basis of elementary experiments with the neat PEEK material. The RVE model for composite material under plane strain conditions with transversal loading has been developed. It was found that overestimation of strain at failure for composite material can be explained well by the manufacturing shrinkage of the matrix. The value of 3% for PEEK shrinkage was chosen as effective one to realize required residual stresses in the composite material. The combination of provided material model with initial manufacturing stresses gives well approximation for macro-level experiment.

Acknowledgments

The research was supported by the Russian Science Foundation (Grant No. 20-11-20230).

REFERENCES

[1] Pinho, S.T., Iannucci, L., Robinson, P. (2006). Physically-based failure models and criteria for laminated fibre-reinforced composites with emphasis on fibre kinking: Part I: Development, Compos. Part A Appl. Sci. Manuf., 37(1), pp. 63–73. DOI: 10.1016/j.compositesa.2005.04.016.

[2] Vogler, M., Rolfes, R., Camanho, P.P. (2013). Mechanics of Materials Modeling the inelastic deformation and fracture of polymer composites – Part I : Plasticity model, Mech. Mater., 59, pp. 50–64. DOI: 10.1016/j.mechmat.2012.12.002.

[3] Asur Vijaya Kumar, P.K., Dean, A., Reinoso, J., Paggi, M. (2021). A multi phase-field-cohesive zone model for laminated composites: Application to delamination migration, Compos. Struct., 276(August), p. 114471. DOI: 10.1016/j.compstruct.2021.114471.

[4] Farmand-Ashtiani, E., Alanis, D., Cugnoni, J., Botsis, J. (2015). Delamination in cross-ply laminates: Identification of traction-separation relations and cohesive zone modeling, Compos. Sci. Technol., 119, pp. 85–92. DOI: 10.1016/j.compscitech.2015.09.025.

[5] Chen, B.Y., Tay, T.E., Pinho, S.T., Tan, V.B.C. (2017). Modelling delamination migration in angle-ply laminates, Compos. Sci. Technol., 142, pp. 145–155. DOI: 10.1016/j.compscitech.2017.02.010.

[6] Zhao, L., Wang, Y., Zhang, J., Gong, Y., Hu, N., Li, N. (2017). XFEM-based model for simulating zigzag delamination growth in laminated composites under mode I loading, Compos. Struct., 160, pp. 1155–1162. DOI: 10.1016/j.compstruct.2016.11.006.

[7] Li, X., Chen, J. (2016). An extended cohesive damage model for simulating multicrack propagation in fibre composites, Compos. Struct., 143, pp. 1–8. DOI: 10.1016/j.compstruct.2016.02.026.

[8] Hu, X.F., Lu, X., Tay, T.E. (2018). Modelling delamination migration using virtual embedded cohesive elements formed through floating nodes, Compos. Struct., 204(July), pp. 500–512. DOI: 10.1016/j.compstruct.2018.07.120.

[9] Vignoli, L.L., Savi, M.A., Pacheco, P.M.C.L., Kalamkarov, A.L. (2019). Comparative analysis of micromechanical models for the elastic composite laminae, Compos. Part B Eng., 174(March), p. 106961. DOI: 10.1016/j.compositesb.2019.106961.

[10] Melro, A.R., Camanho, P.P., Pinho, S.T. (2008). Generation of random distribution of fibres in long-fibre reinforced composites, Compos. Sci. Technol., 68(9), pp. 2092–2102. DOI: 10.1016/j.compscitech.2008.03.013.

[11] Wang, W., Dai, Y., Zhang, C., Gao, X., Zhao, M. (2016). Micromechanical Modeling of Fiber-Reinforced Composites with Statistically Equivalent Random Fiber Distribution, Materials (Basel)., 9(8), pp. 1–14. DOI: 10.3390/ma9080624.

[12] Tyrus, J.M., Gosz, M., Desantiago, E. (2007). A local finite element implementation for imposing periodic boundary conditions on composite micromechanical models, 44, pp. 2972–2989. DOI: 10.1016/j.ijsolstr.2006.08.040.

[13] Tan, W., Naya, F., Yang, L., Chang, T., Falzon, B.G., Zhan, L., Molina-Aldareguía, J.M., González, C., Llorca, J. (2018). The role of interfacial properties on the intralaminar and interlaminar damage behaviour of unidirectional composite laminates: Experimental characterization and multiscale modelling, Compos. Part B Eng., 138(April 2017), pp. 206–221. DOI: 10.1016/j.compositesb.2017.11.043.

[14] Sun, Q., Zhou, G., Meng, Z., Guo, H., Chen, Z., Liu, H., Kang, H., Keten, S., Su, X. (2019). Failure criteria of unidirectional carbon fiber reinforced polymer composites informed by a computational micromechanics model, Compos. Sci. Technol., 172. DOI: 10.1016/j.compscitech.2019.01.012.

[15] Chen, J., Wan, L., Ismail, Y., Hou, P., Ye, J., Yang, D. (2021). Micromechanical analysis of UD CFRP composite lamina under multiaxial loading with different loading paths, Compos. Struct., 269(October 2020), p. 114024. DOI: 10.1016/j.compstruct.2021.114024.

[16] Yuan, K., Liu, K., Zhao, M., Wei, K., Wang, Z. (2022). The in situ matrix cracking behavior in cross-ply laminates under out-of-plane shear loading, Compos. Struct., 290(April), p. 115563. DOI: 10.1016/j.compstruct.2022.115563.

[17] Sepasdar, R., Shakiba, M. (2022). Micromechanical study of multiple transverse cracking in cross-ply fiber-reinforced composite laminates, Compos. Struct., 281(September 2021), p. 114986. DOI: 10.1016/j.compstruct.2021.114986.

[18] Varandas, L.F., Arteiro, A., Catalanotti, G., Falzon, B.G. (2019). Micromechanical analysis of interlaminar crack propagation between angled plies in mode I tests, Compos. Struct., 220(April), pp. 827–841. DOI: 10.1016/j.compstruct.2019.04.050.

[19] Shariyat, M. (2022). Novel 2D strain-rate-dependent lamina-based and RVE/phase-based progressive fatigue damage criteria for randomly loaded multi-layer fiber-reinforced composites, Frat. Ed Integrita Strutt., 16(59), pp. 423–443. DOI: 10.3221/IGF-ESIS.59.28.

[20] Breiman, U., Meshi, I., Aboudi, J., Haj-Ali, R. (2022). Finite strain PHFGMC micromechanics with damage and failure, Acta Mech., 233(7), pp. 2615–2651. DOI: 10.1007/s00707-022-03239-x.

[21] Gao, S.L., Kim, J.K. (2000). Cooling rate influences in carbon fibre/PEEK composites. Part 1. Crystallinity and interface adhesion, Compos. Part A Appl. Sci. Manuf., 31(6), pp. 517–530. DOI: 10.1016/S1359-835X(00)00009-9.
[22] Gillespie, J.W., Chapman, T.J. (1993). The Influence of Residual Stresses on Mode I Interlaminar Fracture of Thermoplastic Composites, J. Thermoplast. Compos. Mater., 6(2), pp. 160–174. DOI: 10.1177/089270579300600206.
[23] Fedulov, B.N., Bondarchuk, D.A., Fedorenko, A.N., Lomakin, E. V. (2022). Residual stresses near the free edge of composite materials, Acta Mech., 233(2), pp. 417–435. DOI: 10.1007/s00707-021-03113-2.
[24] Fedulov, B.N. (2018). Modeling of manufacturing of thermoplastic composites and residual stress prediction, Aerosp. Syst., 1(2), pp. 81–86. DOI: 10.1007/s42401-018-0018-8.
[25] Bondarchuk, D.A., Fedulov, B.N., Fedorenko, A.N., Lomakin, E. V. (2019). The analysis of residual stresses in layered composites with [0°/90°] layup, PNRPU Mech. Bull., 2019(3), pp. 17–26. DOI: 10.15593/perm.mech/2019.3.02.
[26] Li, N., Chen, P.H., Ling, X. (2020). A microscopic elasto-plastic damage model for characterizing transverse responses of unidirectional fiber-reinforced polymer composites, Thin-Walled Struct., 154. DOI: 10.1016/j.tws.2020.106828.
[27] Vaughan, T.J., McCarthy, C.T. (2011). Micromechanical modelling of the transverse damage behaviour in fibre reinforced composites, Compos. Sci. Technol., 71(3), pp. 388–396. DOI: 10.1016/j.compscitech.2010.12.006.
[28] Solvay, APC-2 PEEK Datasheet. (2017).
Available online: https://www.solvay.com/en/product/apc-2peeks2 (accessed on 1 July 2022).
[29] Cytec, Technical data sheet apc-2-peek thermoplastic polymer
https://www.cytec.com/sites/default/files/datasheets/APC-2_PEEK_031912-01.pdf (accessed on 1 July 2022).
[30] Fedulov, B.N., Safonov, A.A., Kantor, M.M., Lomov, S. V. (2017). Modelling of thermoplastic polymer failure in fiber reinforced composites, Compos. Struct., 163, pp. 293–301. DOI: 10.1016/j.compstruct.2016.11.091.
[31] Burdukovsky, V. G., Kolmogorov, V. L. and Migachev, B. A. (1995). Prediction of resources of materials of machine and construction elements in the process of manufacture and exploitation. Journal of materials processing technology, 55(3-4), 292-295. DOI: 10.1016/0924-0136(95)02020-9
[32] Hooputra, H., Gese, H., Dell, H., Werner, H. (2004). A comprehensive failure model for crashworthiness simulation of aluminium extrusions, Int. J. Crashworthiness, 9(5), pp. 449–463. DOI: 10.1533/ijcr.2004.0289.
[33] Lawrence, W.E., Seferis, J.C., Gillespie, J.W. (1992). Material response of a semicrystalline thermoplastic polymer and composite in relation to process cooling history, Polym. Compos., 13(2), pp. 86–96. DOI: 10.1002/pc.750130204.